Mesoscopic superconducting disks

P. Singha Deo*, F. M. Peeters**, and V. A. Schweigert^o
Department of Physics, University of Antwerp (UIA), B-2610 Antwerpen, Belgium.

Using the non-linear Ginzburg-Landau (GL) eqs. type I superconducting disks of finite radius (R) and thickness (d) are studied in a perpendicular magnetic field. Depending on R and d, first or second order phase transitions are found for the normal to superconducting state. For sufficiently large R several transitions in the superconducting phase are found corresponding to different angular momentum giant vortex states. In increasing magnetic field the superconductor is in its ground state, while in field down sweep it is possible to drive the system into metastable states. We also present a quantitative analysis of the relation between the detector output and the sample magnetization. The latter, and the incorporation of the finite thickness of the disks, are essential in order to obtain quantitative agreement with experiment.

PACS numbers: 74.25.Ha; 74.60.Ec; 74.80.-g

I. INTRODUCTION

Superconductivity is one of the most well studied phenomena in condensed matter physics. Superconductivity in bulk samples, thin films, cylinders and hollow cylinders have been extensively studied and can even be found in text books [1]. With the advent of nano-fabrication technologies, there is revived interest in superconductivity in mesoscopic samples [2-10] and to investigate the effect of the geometry and the size of the sample in the superconducting state. Mesoscopic samples are defined as samples whose size is comparable to the coherence length. Moschalkov *et al* [11] measured the superconducting-normal phase diagram of a mesoscopic superconducting square and rectangular ring. They used resistivity measurements which does not allow for probing deep inside the superconducting state. Furthermore, the presence of conduction probes may influence the superconducting state of the studied sample. In order to circumvent these limitations one needs a contactless experiment which is provided by a magnetization measurement. Buisson *et al* [12] performed magnetization measurements on an ensemble of In disks with large separation between them in order to make the dipolar interaction between the disks negligible. Recently Geim *et al* [13] used sub-micron Hall probes to detect the magnetization of *single* superconducting Al disks with size down to 0.1 μm. These experimental works are the main motivation behind our present and previous theoretical work.

Already a substantial amount of theoretical work has been done on mesoscopic samples using the Ginzburg-Landau (GL) theory. Some of these works neglect the non-linear term in the first GL eqn [2,9,12]. But all these works neglect the de-magnetization effect which arises due to the finite thickness of the disk [3–5,7,8,10]. The latter is very important in case there is a substantial Meissner effect and is the reason for the discrepancies between the experimental observations and the existing theories. For example, Buisson *et al* [12] observed an oscillatory behavior (or jumps) in the magnetization which occurs above a certain applied magnetic field. Linearized Ginzburg-Landau (LGL) theory could explain the origin of the oscillatory behavior, but is not able to explain: *i*) the magnetic field above which the oscillations occur, *ii*) its amplitude, and *iii*) the periodicity of these oscillations. Hence they questioned the validity of the GL theory in dealing with the magnetization of mesoscopic samples. Such oscillatory behavior has also been obtained in the single disk measurement of Geim *et al.* [13], provided the disk is large enough to accommodate many flux quanta. Ref. [13] showed that the very nature of the normal to superconductor transition can change from a first order phase transition to a second order as the dimensions of the disk is varied. Notice that bulk Al has $\xi(0) = 1.6\mu m$, $\lambda(0)=.016\mu m$ and consequently the GL parameter is $\kappa=0.01$ which tells us that Al is a type I sample and consequently the superconducting to normal transition is first order in that case.

We showed recently that the GL theory can explain the magnetic field at which the oscillations start, the amplitude of the oscillations and the periodicity of the oscillations, provided the non-linear term and the de-magnetization effect are included in the theoretical description [14,15].

The GL theory does not have a firm mathematical derivation except in a narrow range of magnetic field close to the phase boundary of type II bulk materials [16]. However because of its simplicity, it enables us to make quantitative calculations for most of the experimentally observed quantities, which makes it a popular theory. From experience it is known that it gives sensible results even beyond this limited regime. For example it was found to work for type I thin films [17]. The reason is that thin films are governed by an effective penetration length $\lambda_e = \lambda^2/d$ which results in an effective GL penetration length larger than $1/\sqrt{2}$. Surface superconductivity or the giant vortex state could be quantitatively understood from the GL theory for samples with boundaries [18]. The phase boundary of mesoscopic type I samples could be quantitatively explained from the GL theory [11]. Refs. [14,15,19] applied the GL theory to study the magnetization of mesoscopic disks deep inside the phase boundary and there was remarkable quantitative agreement with the experimental observations.

In the present work the GL approach to disks is reviewed and the non-linear Meissner effect is analyzed in detail. We show that the detector size greatly influences the measured magnetization. In smaller disks it only influences the magnitude whereas in larger disks it can influence both the magnitude as well as the line shape. Thus we find that one has to be careful to translate the measured Hall voltage directly into the sample magnetization. Also the hysteresis behavior of the magnetization will be analyzed in detail.

II. THEORETICAL TREATMENT

We consider superconducting disks with radius R and thickness d immersed in an insulating medium. As a first approximation, neglecting the non-local effects, we solve the system of two coupled GL eqns.

$$\frac{1}{2m}\left(-i\hbar\vec{\nabla}-\frac{2e\vec{A}}{c}\right)^2\Psi=-\alpha\Psi-\beta\Psi|\Psi|^2, \tag{1}$$

$$\vec{\nabla}\times\vec{\nabla}\times\vec{A}=\frac{4\pi}{c}\vec{j}, \tag{2}$$

where the density of superconducting current $\vec{j}$ is given by

$$\vec{j}=\frac{e\hbar}{im}\left(\Psi^*\vec{\nabla}\Psi-\Psi\vec{\nabla}\Psi^*\right)-\frac{4e^2}{mc}|\Psi|^2\vec{A}. \tag{3}$$

Here α is a temperature dependent parameter: $\alpha=\alpha(0)(T/T_c-1)$ while β is regular at T_c, where T_c is the critical temperature. On the disk surface we require that the normal component of the current density is zero

$$\left(-i\hbar\vec{\nabla}-\frac{2e\vec{A}}{c}\right)_n\Psi=0, \tag{4}$$

The boundary condition for the vector potential is such that far away from the superconducting disk the field equals the applied field $\vec{H}=(0,0,H_0)$, i.e., $\vec{A}|_{\vec{\rho}\to\infty}=\vec{e}_\phi H_0\rho/2$. Here $\vec{e}_\phi$ denotes the azimuthal direction and ρ is the radial distance from the disk center.

Using the London gauge $div\vec{A}=0$, we rewrite the system of eqns. (1-3) into the following form

$$\left(-i\vec{\nabla}-\vec{A}\right)^2\Psi=\Psi(1-|\Psi|^2), \tag{5}$$

$$-\kappa^2\triangle\vec{A}=\frac{1}{2i}\left(\Psi^*\vec{\nabla}\Psi-\Psi\vec{\nabla}\Psi^*\right)-|\Psi|^2\vec{A}, \tag{6}$$

where distance is measured in units of the coherence length $\xi=\hbar/\sqrt{-2m\alpha}$, the order parameter in $\psi_0=\sqrt{-\alpha/\beta}$, the vector potential in $c\hbar/2e\xi$, $\kappa=\lambda/\xi$ is the GL parameter, and $\lambda=c\sqrt{m/\pi}/4e\psi_0$ is the bulk penetration length. We measure the magnetic field in $H_{c2}=c\hbar/2e\xi^2=\kappa\sqrt{2}H_c$, where $H_c=\sqrt{-4\pi\alpha/\beta}$ is the bulk critical field. Notice that the parameters α and β are scaled out of the GL equations and consequently they only determine the energy and length scales.

The difference of the Gibbs free energy G between the superconducting and the normal state, measured in $H_c^2V/8\pi$, can be expressed through the integral

$$G=\int\left(2(\vec{A}-\vec{A}_0).\vec{j}-|\Psi|^4\right)d\vec{r}/V, \tag{7}$$

over the disk volume $V=\pi R^2d$, where $\vec{A}_0=\vec{e}_\phi H_0\rho/2$ is the external vector potential, and $\vec{j}=(\Psi^*\vec{\nabla}\Psi-\Psi\vec{\nabla}\Psi^*)/2i-|\Psi|^2\vec{A}$ is the dimensionless superconducting current. The magnetization is defined as

$$M=\int_S(H_z-H_0)d\vec{r}/4\pi, \tag{8}$$

which is a direct measure of the expelled magnetic field from the surface area S of the disk.

We used the Gauss-Seidel method to solve Eqn. 1 and the fast Fourier transform to solve Eqn 2. The order parameter of the previous magnetic field is taken as the initial order parameter for a particular magnetic field. A large number of iterations are then made to arrive at a self consistent solution. In previous work we found that the assumption that the order parameter is uniform in the z-direction is a very good approximation for the thin disks considered here [6,14,15]. Consequently, as far as the order parameter is concerned the disk is reduced to a 2D disk. But the 3D nature of the field distribution is completely retained. Hence Eqs. 1 and 2 becomes

$$\left(-i\vec{\nabla}_{2D}-\vec{A}\right)^2\Psi=\Psi(1-|\Psi|^2), \tag{9}$$

$$-\triangle_{3D}\vec{A}=\frac{d}{\kappa^2}\delta(z)\vec{j}_{2D}, \tag{10}$$

$$\vec{j}_{2D}=\frac{1}{2i}\left(\Psi^*\vec{\nabla}_{2D}\Psi-\Psi\vec{\nabla}_{2D}\Psi^*\right)-|\Psi|^2\vec{A}, \tag{11}$$

with the boundary condition $(-i\vec{\nabla}_{2D}-\vec{A})_n\Psi|_{r=R}=0$.

It is known that for superconducting cylinders, the sample can only exhibit the Abrikosov vortex state when the GL parameter $\kappa>1/\sqrt{2}$. This is no longer so for thin disks, because they have an *effective* κ which is much different from that of cylinders. Outside the Abrikosov vortex state region, both the Meissner state and the giant vortex state have azimuthal symmetry. Hence for a disk that does not exhibit the multi-vortex state [19], we can assume axially symmetric solutions with a general angular momentum: $\Psi(\vec{\rho})=F(r)exp(iL\phi)$. This will reduce the dimensions of Eqs. 1 and 2 and thus it greatly improves the computation time and the accuracy. For simplicity we will refer to the first method as 3D solution and the second method with fixed L as 2D solution.

III. GROUND STATE AND METASTABILITY IN MESOSCOPIC SUPERCONDUCTING DISKS

As a typical case let us consider a disk of radius R=0.8μm, thickness d=0.134 μm, coherence length $\xi(0)$=0.183 μm and penetration length $\lambda(0)$=0.07μm (resulting in $\kappa = 0.383$) which are comparable to those of one of the Al disks considered in the experiment of Geim *et al* [13]. In the case of the 2D solution we solve for a particular L state. The transition between the different L states is obtained from a comparison of the free energies from which we obtain the ground state. The free energy G as a function of increasing applied magnetic field is shown by the thin solid curves in Fig. 1(a) for different L states. The corresponding magnetization are shown in Fig. 1(b) by the thin solid curves. Hence from Fig. 1(a), it can be seen that up to a magnetic field of 42.6 Gauss, the L=0 state is the ground state. Beyond this field the L=1 state becomes the ground state. As we increase the field, higher L states become the lowest energy states. This continues as long as the free energy G is negative. A positive G means that the normal state has a lower free energy than the superconducting state. Hence the free energy of the ground state of the system is given by the thick solid curve in Fig. 1(a). The corresponding magnetization along this ground state is given by the thick solid curve in Fig. 1(b). Notice that each L state has a metastable region where the sample can be paramagnetic.

The 3D approach does not have the restriction of fixed L and consequently many solutions can be found for given magnetic field which are not necessarily the lowest energy state. Our approach is to start at zero magnetic field, find the ground state, and then increase the magnetic field in small steps in which we use the order parameter of the previous magnetic field as the initial state in the iteration of the coupled set of differential equations. The magnetization as given by the 3D solution in increasing magnetic field is given by the thick dotted curve in Fig. 1(b). The corresponding free energy is given by the thick dotted curve in Fig. 1(a). As compared to the 2D solution we find that (within errors arising due to the assumption that the order parameter is uniform in the disk in the z-direction in case of the 3D solution), the 3D solution in increasing magnetic field, takes the system along a state that conserves L. This persists up to the point where the L=0 state is no longer metastable, i.e. it no longer has a local minimum. Then the system jumps to the L=1 state and starts evolving along the L=1 state until it is no longer stable. Following the 2D solution along a path of conserving L we notice that the line shape of the magnetization and the number and position of jumps in the magnetization are similar to those of the 3D solution. The little difference in magnitude arises due to the fact that the 3D solution uses the extra approximation of constant order parameter in the z-direction while the order parameter should be reduced near the upper and lower surfaces of the disk. Hence an important conclusion that can be made from the comparison of the 2D solution and the 3D solution is that the 2D solution can be used to study the magnetization of this sample.

Comparing the thick dotted curve in Fig. 1(a) (3D solution) with the thick solid curve in Fig. 1(a) (the ground state obtained from 2D solution) we find that the 3D solution in increasing magnetic field makes the system evolve along metastable states. In the 3D solution the metastability is due to energy barriers which do not allow the sample to switch between different angular momentum states. In the Ginzburg-Landau theory there are two such energy barriers. One of them is a surface barrier known as the Bean-Livingston barrier [20] that has been well studied in the case of cylinders. The other barrier is a volume barrier and it appears only when the sample makes a first order transition to the normal state. This appears because close to the first order transition the free energy has two minima corresponding to two different values of the order parameter and there is a barrier separating the two minima. These two barriers make the system evolve along metastable paths. Therefore, the question arises: what makes the system evolve along the ground state in increasing magnetic fields? The volume barriers in these disks are negligibly small for transitions between different L states of the disk considered in Fig. 1 because in such a case the order parameter on the average changes by a small amount or the local minima are very close to each other. And as is known for cylinders, the surface barrier in increasing fields (but not in decreasing fields) can be destroyed by small surface defects. The disks used in the experiment of Ref [13] have a rough boundary and therefore in increasing field the sample evolves along the ground state.

The situation is different in decreasing field. The surface barrier does not disappear due to surface defects and so in decreasing field the sample will evolve along metastable states, thus resulting in hysteresis. In our model the barriers are present but what is not present are the thermal fluctuations in the system. To a first approximation we can neglect these effects because of the extreme low temperature at which the experiments are done and study hysteresis effects arising due to metastability alone. The result in decreasing field using our 3D solution is given by the thick dashed curves in Fig. 1.

IV. EFFECT OF THE DETECTOR SIZE ON THE MEASUREMENT OF MAGNETIZATION

The magnetometry used in the experimental work of Ref. [13] is explained in detail in Refs. [21]. The superconducting sample is mounted on top of a small Hall cross. From the Hall resistance one can estimate how much field is expelled from the Hall cross, which is due to the expulsion of the field by the superconductor. The Hall cross has a larger area than the sample and it measures the

magnetization of this area rather than the sample. In Ref. [22] it was shown that the Hall voltage of a Hall bar, in the ballistic regime, is determined by the average magnetic field piercing through the Hall cross region. Due to the depletion of the two dimensional electron gas near the edges of the leads of the Hall cross the effective area of the Hall cross is not exactly known and may be smaller than the optical size. Since the field distribution in case of thin disks is extremely non-uniform inside as well as outside the disks (this is essentially different for cylinders where the magnetic field outside the sample always equals the applied field) the detector size will have an effect on the measured magnitude of the magnetization. Since the field just outside the disk is larger than the applied field, a larger detector will underestimate the magnetization, the nature and extent will depend on the field profile outside the disk.

To understand these effects we calculate the magnetization of an area larger than that of the sample by integrating the field expelled from this area. We take a disk of radius 0.44 μm, thickness = 0.15 μm, coherence length $\xi(0) = 0.275$ μm and penetration length $\lambda(0) = 0.07$ μm at T=0.4K. In Fig. 2 we plot the calculated flux expulsion from the sample (solid curve), and from a square area larger (width 1.75 μm, dashed curve) and smaller (width .067 μm, dotted curve) than the sample size. The detector area is taken immediately under the sample. When the detector width is larger than the diameter of the sample, increase of the detector width simply scales down the magnetization. When the detector width is smaller than the diameter of the sample there is a small change in the line shape. The dashed curve when multiplied by 15.83 practically coincides with the solid curve, whereas the dotted curve when scaled by 0.5291 goes over to the dash-dotted curve.

In Fig. 3 we show how the scale factor (defined as peak value of magnetization for a certain detector width divided by the peak value of the sample magnetization) scales with the width w of the detector. The magnetic field profile (applied field + field due to the magnetization of the sample) for a disk of radius $0.44\mu m$ is shown in the lower inset. From this profile it is clear that increasing the detector size w will result in an average magnetic field closer to the applied field and consequently a smaller measured field expulsion and consequently a smaller magnetization. The scale factor shown in Fig. 3 could be fitted to a Gaussian curve with center at 0.18, width of 0.93, height of 1.83 and offset of 0.055. Since the magnetic field is also non-uniform in the z-direction, the magnetization measurement will also be affected by the distance of the detector from the sample. We take a square detector whose width is equal to the diameter of the sample and place it at different distances below the sample. In this case there is no change in line shape and the different curves can be made to coincide with each other by appropriate scaling. In the upper inset of Fig. 3 we show how the scale factor varies with the vertical distance from the middle of the sample. This curve could be fitted to the function $Aexp[(z - z_0)t]$ where A=0.6, z_0=0.07 and t=0.28. In section V we will show that for samples with $L > 1$ the line shape of the magnetization curve can also change with the size and position of the detector but the peak value scales in a similar manner as found in this section. We shall also show that in decreasing fields the conclusions can be very different because magnetization can change sign as a function of w.

V. "FRACTIONAL FLUXOID DISK" AND THE NON-LINEAR MEISSNER EFFECT

If the upper critical field (H_c) of a disk is such that $H_c\pi R^2 < \phi_0$, then we call it a fractional fluxoid disk, where $\phi_0 = hc/2e$ is a single flux quantum. Physically it means that the disk is not large enough to accommodate even a single vortex when in the superconducting state. In such a small disk the L=1 state cannot nucleate and the superconducting state always corresponds to the L=0 state. In this regime the 2D solution is always valid. As an example, we fix the radius of the disk to be 0.3 μm, temperature T=0.4K, coherence length $\xi(0)$=0.25 μm and penetration length $\lambda(0)$=0.07 μm which results in κ=0.28. We plot in Fig. 4 the magnetization versus decreasing applied magnetic field for 5 different thicknesses d. The values of $t = d/\xi(T)$ are shown in the figure where $\xi(T)$=0.31 for T=0.4K. It can be seen that for $t \leq$0.3 the disk shows a second order phase transition to the normal state, whereas for $t \geq$0.5, we find a first order phase transition to the normal state. The magnetization (multiplied by 0.5) from the LGL theory is shown by the dashed curve for the same radius and coherence length. The magnetization for a cylinder in decreasing magnetic field for the same radius and material parameters is shown by the dash-dotted curve. Notice that for very small thickness t the sample shows a second order transition between the normal-superconducting state but as the thickness increases, beyond a critical thickness of t=0.33, this becomes a first order transition. The magnitude of the jump of the magnetization ΔM versus t at the superconducting-normal transition point is shown in Fig. 5. This result can be fitted, (solid curve) to the function $A|t - t_c|^p$, where $A = 2.87 \pm 0.07$, $t_c = .33$ and $p = 0.56 \pm 0.02$. In the inset we plot the peak position of the magnetization curve versus t which we could fit to the function $a + bt^c$ where $a = 55.40 \pm 1.05$, $b = 43.91 \pm 0.99$ and $c = 0.59 \pm 0.03$. It is generally believed that the upper critical field is given accurately by the LGL theory which we find to be true in decreasing magnetic fields.

The same results in increasing magnetic field is given in Fig. 6 where curve conventions are the same as in Fig. 4. In increasing magnetic field the LGL theory gives the correct upper critical field as long as the sample shows a second order transition to the normal state. In this case the upper critical field is independent of the thickness. As the sample starts showing a first order transition the

upper critical field starts increasing with increasing thickness. The reason behind this qualitative difference with the LGL theory in increasing and decreasing field arises due to the fact that in the LGL theory there is only one minimum in the free energy whereas in the GL theory, when the sample shows a second order transition, there is one minimum but when it shows a first order transition, there are two minima in the free energy (the first minimum is at zero order parameter and the second minimum is at a finite order parameter). One of them is however metastable and we shall soon find that the experimental system can exist in such a metastable state. In this case ΔM versus t is shown in Fig. 7. It fits to a function $A(t-t_c)^p$ where $A = 2.16$, t_c=0.33 and p=0.58.

From Figs. 4 and 6 we can understand why a disk can show a first order or a second order phase transition to the normal state as is found in the experiment. It also explains why a fractional fluxoid disk in case of a first order transition shows a different behavior in increasing and decreasing magnetic fields and as a result a remarkable hysteresis as seen in the experiment. In Fig. 8, we show that a disk of radius R=0.44 μm, thickness d=0.15 μm, coherence length $\xi(0)$=0.275 μm and penetration length $\lambda(0)$=0.07 μm at T=0.4K can exhibit a magnetization like that of a disk whose magnetization was measured in the experiment and whose radius was reported as 0.5 μm, thickness between 0.07 μm and 0.15 μm, coherence length of 0.25 μm and penetration length of 0.07 μm. Note that we decrease the coherence length by 10 % and the radius by 12 % to reproduce the experimental result which are well within the errors of experimental estimates. The increasing field behavior as seen in the experiment is given by the open squares and the decreasing field behavior is given by the open circles. Our numerical calculation of the magnetization in increasing and decreasing magnetic field for a detector area of 2.5 μm placed 0.15 μm below the sample is shown by the solid and dotted curves, respectively. The inclusion of the detector size and position results in a magnetization which is a factor 50.44 smaller than the pure sample magnetization. The inset shows the dimensionless free energy as a function of the magnetic field. The dashed line in Fig. 8 is the behavior expected in the case of a linear Meissner effect and is drawn tangential to the small field magnetization curve. Notice that even in the intermediate magnetic field region the magnetization is substantially non-linear. Note that in decreasing field the position of the jump does not agree with the experiment. In case of a first order transition the free energy has two minima separated by a barrier and when the system tries to switch from one minima to the other it has to overcome this barrier. The position of the jump given here corresponds to the situation when this barrier disappears. But due to fluctuations in the system the jump can be at lower fields.

The field distribution along a radial line starting from the center of the disk is shown in Fig. 9(a). The center of the disk is at the origin of the coordinates. Notice that the field is minimum at the center of the disk. It increases drastically with distance from the center and becomes maximum at 0.44 μm which is precisely the radius of the disk. This implies that the field is strongly expelled from the center of the disk. The 11th curve (applied field=70.86 Gauss) corresponds to the critical field at which superconductivity has disappeared.

Magnetization measurement on bulk samples and large radius cylinders shows that in the pure "Meissner state", the sample behaves as a perfect diamagnet which means magnetization is proportional to the applied field with a susceptibility (χ=$4\pi M$/H) of -1. This experimental observation led to the well known London theory. It can already be seen from the magnetization measurement (see the experimental data in Fig. 8) that London theory is not valid for the present disks because of the non-linear magnetization versus the applied field. Even in the small field region the susceptibility is much smaller than -1 because of large field penetration in a finite size sample as can be seen from Fig. 9(a). In the usual London approach the field penetration is determined by the field value at the boundary of the sample. In Fig. 9(b) we show the normalized field distribution, i.e., the field is divided by its maximum value which is found at the edge of the disk. This helps us to compare the field penetration at different applied fields. For small applied fields (say less than 25 G) the curves fall on top of each other as expected from London theory. But for larger applied fields the field penetration is no longer only determined by the field at the boundary of the disk and becomes substantially larger. In the inset of Fig. 9(b) we plot the magnetic field normalized to the applied field.

VI. FEW FLUXOID DISKS

When a disk is large enough to accommodate one or more fluxoids we call it a "few fluxoid disk". Unlike for "fractional fluxoid disk", for the "few fluxoid disk" case the LGL and GL theories give qualitatively similar result. The upper critical field and the number of jumps in the magnetization is the same in both theories. But in order to explain the position and the magnitude of the jumps it is necessary to consider the full GL eqns. To explain the increasing field behavior we assume that the system remains in the ground state, which can be determined from the 2D solution as explained in section III.

Fig. 10(a) shows the magnetization of a few fluxoid disk: the open circles are the experimental data (at T=0.4 K) plotted according to the scale on the left axis. The experimental estimates of radius is 0.75 μm, thickness is between 0.07 μm to 0.15 μm, coherence length is 0.25 μm and penetration length is 0.07 μm. Sample magnetization along the ground state calculated from our 2D solution is shown by the dashed curve and it is plotted according to the scale on the right. Parameter values used for the radius is 0.8 μm, thickness is 0.134 μm,

temperature is 0.4 K, coherence length is 0.183 μm and penetration length is 0.07 μm. There is a factor of 25 difference in the magnitude of magnetization. However when we use a detector of width 3 μm placed 0.15 μm below the sample, the ground state magnetization, as defined by the flux expulsion from the detector square, is given by the solid curve plotted according to the scale on the left. Notice that the inclusion of the detector effect explains the magnitude of magnetization and it also changes slightly the slope of the curve for fields larger than 40 G. Namely the magnetization decreases faster with magnetic field.

Also the magnetization in decreasing magnetic field is shown in Fig. 10(b) where the curve conventions are the same as for the field sweep up. It is needless to say that the agreement with the experimental data is remarkable except for the last jump at low field. In Fig. 11 we show how the minimum magnetization at 55.795 Gauss scales with the size of the detector in case of the field down sweep. For detector size smaller than the sample the magnetization is strongly paramagnetic due to the pinned fluxoid in the sample. Also when the detector size slightly exceeds the sample size the magnetization can be paramagnetic which decrease as the detector size is made larger.

Next in Fig. 12 we consider an even larger disk which is able to contain 19 flux quanta before it becomes normal. The experimental data of magnetization versus increasing magnetic fields at T=0.4 K is shown by the open circles according to the scale on the left. The experimental estimate of the parameters are radius=1.2 μm, thickness is between 0.07 μm and 0.15 μm. Our 2D solution for the ground state magnetization of the sample is shown by the dashed curve according to the scale on the right. Parameter values used for radius is 1.25 μm, thickness is 0.136 μm, coherence length is 0.195 μm and penetration length is 0.07 μm. When we use a detector of width 4 μm placed 0.15 μm below the sample the ground state magnetization is given by the solid curve. Note that the size of the detector used here appears to be a bit larger than expected experimentally. Using a detector of smaller width does not appreciably change the line shape as long as it is slightly larger than the disk diameter. Also the convex shape of the curve for field larger than 25G is recovered although it is less than that found experimentally. Note that the position of the first jump, the upper critical field and the total number of jumps is the same as that found experimentally.

The jumps observed in Figs. 10 and 12 reminds us of the Little Parks oscillations seen in ring shaped superconductors and other multiply connected geometries [11]. In such geometries it occurs due to flux quantization in superconductors and hence these jumps occur at extremely regular intervals (provided the sample is clean). It is to be noted that in Figs. 10 and 12 the interval between jumps is slowly decreasing in the experimental data as well as in the theoretical curve. In Fig. 13(a) we plot the magnetic field interval between two successive jumps, ΔH, versus the angular momentum L for the ground state (open circles) which are compared with the experimental data (solid squares). We find that the experimental ΔH is extremely irregular, which suggests that entry of fluxoids into the sample is hindered by disorder and pinning centers. Another reason may be the experimental accuracy and fluctuations in the applied field which are expected to lead to an error of about 10 % in these quantities. The overall behavior: of a large ΔH for small L and a smaller but constant ΔH for larger L is clearly visible in the experimental result. The open squares in Fig. 13(a) are obtained from the recent theoretical result of Ref. [7]. He used a variational approach to solve the GL equation with the approximation of an uniform magnetic field distribution. His calculation was done for $R = 5.25\xi$ and $\kappa = 1.2$. The origin of this drastic decrease in ΔH arises due to strong flux expulsion and the demagnetization effects at low fields because of which the flux inside the sample increases at a very slow rate as compared to the applied field. So the external field has to be increased by more than a flux quantum to give rise to one flux quantum inside the disk. Such strong flux expulsion becomes weaker as field is increased and becomes zero at the critical field. So at higher fields ΔM versus L becomes flat and corresponds to the flux quantization condition: $\Delta H \pi R^2 = \phi_0$.

In Fig. 13(b) the magnitude of the jumps in the magnetization (ΔM) is shown and compared with the experimental data and the theoretical result of Ref. [7]. The theory gives a substantial larger magnitude of the jumps than seen experimentally except for the smaller radius sample (see inset) when $L > 4$.

VII. CONCLUSIONS

Apart from explaining quantitatively and qualitatively the recent experiments of Geim *et al* we can make some general conclusions. The GL theory captures all the features of mesoscopic superconductors provided the nonlinear term and the field distribution is properly accounted for. Hence it is necessary to review the calculation of various quantities in mesoscopic superconductors made so far which did not account for these effects. We can also conclude that in increasing magnetic fields the sample evolves along the free energy minimum and the Bean-Livingston barrier plays no role. Surface defects destroy the Bean-Livingston barrier in increasing fields in the case of cylinders. This also seems to be true for disks. We also find that the magnitude of magnetization is drastically affected by the detector size. The nature of the measured magnetization curves are sensitive to small changes in parameters.

VIII. ACKNOWLEDGMENTS

This work is supported by the Flemish Science Foundation(FWO-Vl) grant No: G.0232.96, the Belgian Inter-University Attraction Poles (IUAP-VI). One of us (PSD) is supported by a post doctoral scholarship from the FWO-Vl and FMP is a Research Director with the FWO-Vl. It is a pleasure to acknowledge stimulating discussions with A. Geim.

---

* Electronic mail: deo@uia.ua.ac.be

** Electronic mail: peeters@uia.ua.ac.be

o Permanent address: Institute of Theoretical and Applied Mechanics, Russian Academy of Sciences, Novosibirsk 630090, Russia.

[1] P. G. de Gennes, *Superconductivity of Metals and Alloys*, (Addison Wesley, New York, 1989).

[2] A. I. Buzdin and J. P. Brison, Phys. Lett. A **196**, 267 (1994).

[3] R. Kato, Y. Enomoto, and S. Maekawa, Phys. Rev. B **47**, 8016 (1993).

[4] C. Bolech, G. C. Buscaglia, and A. López, Phys. Rev. B **52**, 15719 (1995).

[5] V. M. Fomin, V. R. Misko, J. T. Devreese, and V. V. Moschalkov, Solid State Commun. **101**, 303 (1997), *ibid* Phys. Rev. B **58**, 11703 (1998).

[6] V. A. Schweigert and F. M. Peeters, Phys. Rev. B **57**, 13 817 (1998).

[7] J. J. Palacios, Phys. Rev. B **57**, 10 873 (1998).

[8] E. Akkermans and K. Mallick (to be published).

[9] R. Benoist and W. Zwerger, Z. Phys. B **103**, 377 (1997).

[10] V. V. Moshchalkov, X. G. Qiu, and V. Bruyndoncx, Phys. Rev. B **55**, 11793 (1997).

[11] V. V. Moshchalkov, L. Gielen, G. Strunk, R. Jonkheere, X. Qiu, C. van Haesendonck, and Y. Bruynseraede, Nature **373**, 319 (1995).

[12] O. Buisson, P. Gandit, R. Rammal, Y. Y. Wang, and B. Pannetier, Phys. Lett. A **150** 36 (1990).

[13] A. K. Geim, I. V. Grigorieva, S. V. Dubonos, J. G. S. Lok, J. C. Maan, A. E. Filippov and F. M. Peeters, Nature, **390**, 259 (1997).

[14] P. Singha Deo, V. A. Schweigert, F. M. Peeters and A. K. Geim, Phys. Rev. Lett. **79**, 4653 (1997).

[15] P. Singha Deo, V. A. Schweigert, and F. M. Peeters, cond-mat/9804174.

[16] V. L. Ginzburg and L. D. Landau, Zh. Eksperim. i Teor. Fiz. **20**, 1064 (1950); L. P. Gor'kov, Zh. Eksperim. i Teor. Fiz. **36**, 1918 (1959) [Soviet Phys. - JETP **9**, 1364 (1959).

[17] G. Dolan, J. Low Temp. Phys. **15**, 133 (1974).

[18] D. Saint-James and P. G. de Gennes, Phys. Lett. **7**, 306 (1963).

[19] V. A. Schweigert, F. M. Peeters, and P. Singha Deo, Phys. Rev. Lett. **81**, 2783 (1998).

[20] C. P. Bean and J. D. Livingston, Phys. Rev. Lett. **12**, 14 (1964).

[21] A. K. Geim, S. V. Dubonos, I. V. Grigorieva, J. G. S. Lok and J. C. Maan, Appl. Phys. Lett. **72**, 572 (1998).

[22] F. M. Peeters and X. Q. Li, Appl. Phys. Lett. **72**, 572 (1998).

FIGURE CAPTIONS

FIG. 1. Free energy versus increasing magnetic field for different angular momentum (L) states are shown by thin solid curves. Thick solid curve is the free energy versus increasing magnetic field for the ground state of the sample, the thick dotted curve is the result from the 3D solution and the thick dashed curve shows the same for decreasing magnetic fields. Here $G_0 = H_c^2 V/8\pi$. (b) The corresponding magnetization for the curves in (a) with the same convention for the different curves.

FIG. 2. Magnetization versus increasing magnetic field for different detector sizes.

FIG. 3. The scale factor for the magnetization as function of the width of the detector. The upper inset shows how this scale factor varies with the distance of the detector. The lower inset shows how the magnetic field varies along a line from the center of the disk for the particular disk considered in this figure.

FIG. 4. The gradual change from a first order to a second order phase transition as the thickness of a sample is increased. The curves are obtained for decreasing magnetic field sweep.

FIG. 5. ΔM is the magnitude of the jumps in the magnetization seen in Fig. 4. The solid circles give ΔM for the corresponding value of t. The solid curve is a χ^2-fit to it. The inset shows how the peak position of the curves in Fig. 4 vary with t along with a χ^2-fit.

FIG. 6. The gradual change from a first order to a second order phase transition as the thickness of a sample is increased for increasing magnetic field sweep.

FIG. 7. The solid circles give ΔM for the corresponding value of t. The solid curve is χ^2 fit to it. The inset shows how the transition field vary with t along with a χ^2 fit.

FIG. 8. Comparison between experimentally observed magnetization in increasing (open squares) and decreasing fields (open circles) and our numerically calculated magnetization in increasing (solid curve) and decreasing (dotted curve) magnetic field. The dashed curve is a tangent to the experimental data at the origin. The inset shows the dimensionless free energy for the system.

FIG. 9. (a) Magnetic field change from the center of the disk considered in Fig. 8 for different applied fields mentioned in the figure. (b) Magnetic field curves of Fig. 9(a) when scaled by the maximum field for each curve. The inset shows the magnetic field when scaled by the applied field.

FIG. 10. (a) Comparison between experimentally observed magnetization in increasing (open circles) fields according to the scale on the left y-axis and our numerically calculated magnetization in increasing (dashed curve) magnetic field according to the scale on the right y-axis. The solid curve is according to the left y-axis and

is obtained when the detector size is taken into account. (b) The same for decreasing magnetic fields.

FIG. 11. The magnetization of the sample of Fig. 10(b) at 55.795 Gauss as function of the detector size.

FIG. 12. Comparison between experimentally observed magnetization in increasing (open circles) fields according to the scale on the left y-axis and our numerically calculated magnetization in increasing (dashed curve) magnetic field according to the scale on the right y-axis. The solid curve is according to the left y-axis and is obtained when the detector size is taken into account.

FIG. 13. (a) Comparison of experimentally observed and numerically obtained ΔH (magnetic field change due to penetration of one extra fluxoid) versus L for the disk considered in Fig. 12. The solid squares give the experimental data, the open circles are our numerically obtained values and the open squares correspond to the results of Ref. [7]. The curves are guides to the eye. The inset shows the same for the case of Fig. 10(a). (b) Comparison of experimentally observed and numerically obtained ΔM (jumps in the magnetization) versus L for the disk considered in Fig. 12. The symbol conventions are the same as in Fig. 13(a). The inset shows the same for the case of Fig. 10(a).

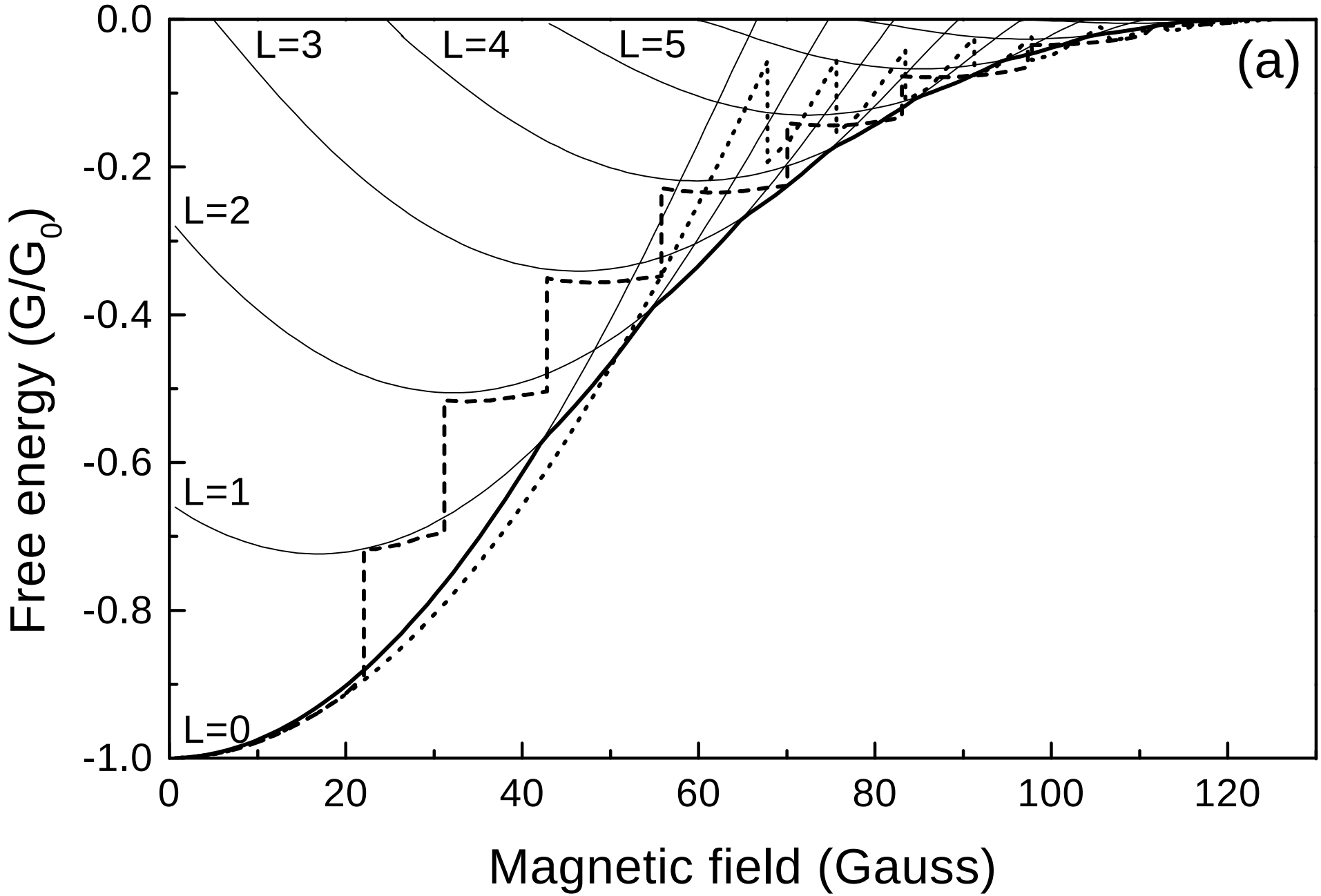
0.0
-0.2
-0.4
-0.6
-0.8
-1.0
0
20
40
60
80
100
120
Free energy (G/G0)
Magnetic field (Gauss)
L=3
L=4
L=5
L=2
L=1
L=0
(a)

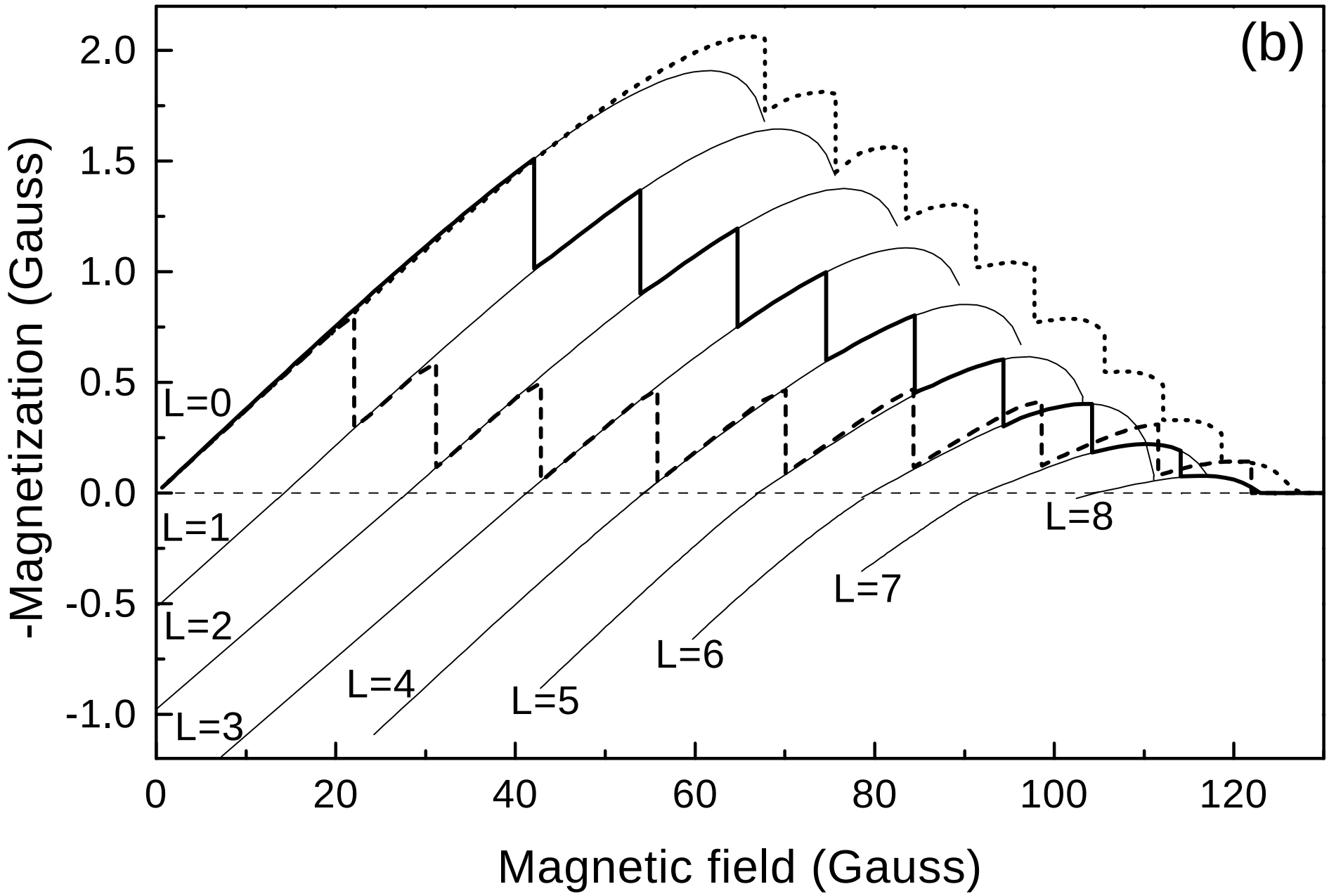
(b)
2.0
1.5
1.0
0.5
0.0
-0.5
-1.0
-Magnetization (Gauss)
0
20
40
60
80
100
120
Magnetic field (Gauss)
L=0
L=1
L=2
L=3
L=4
L=5
L=6
L=7
L=8

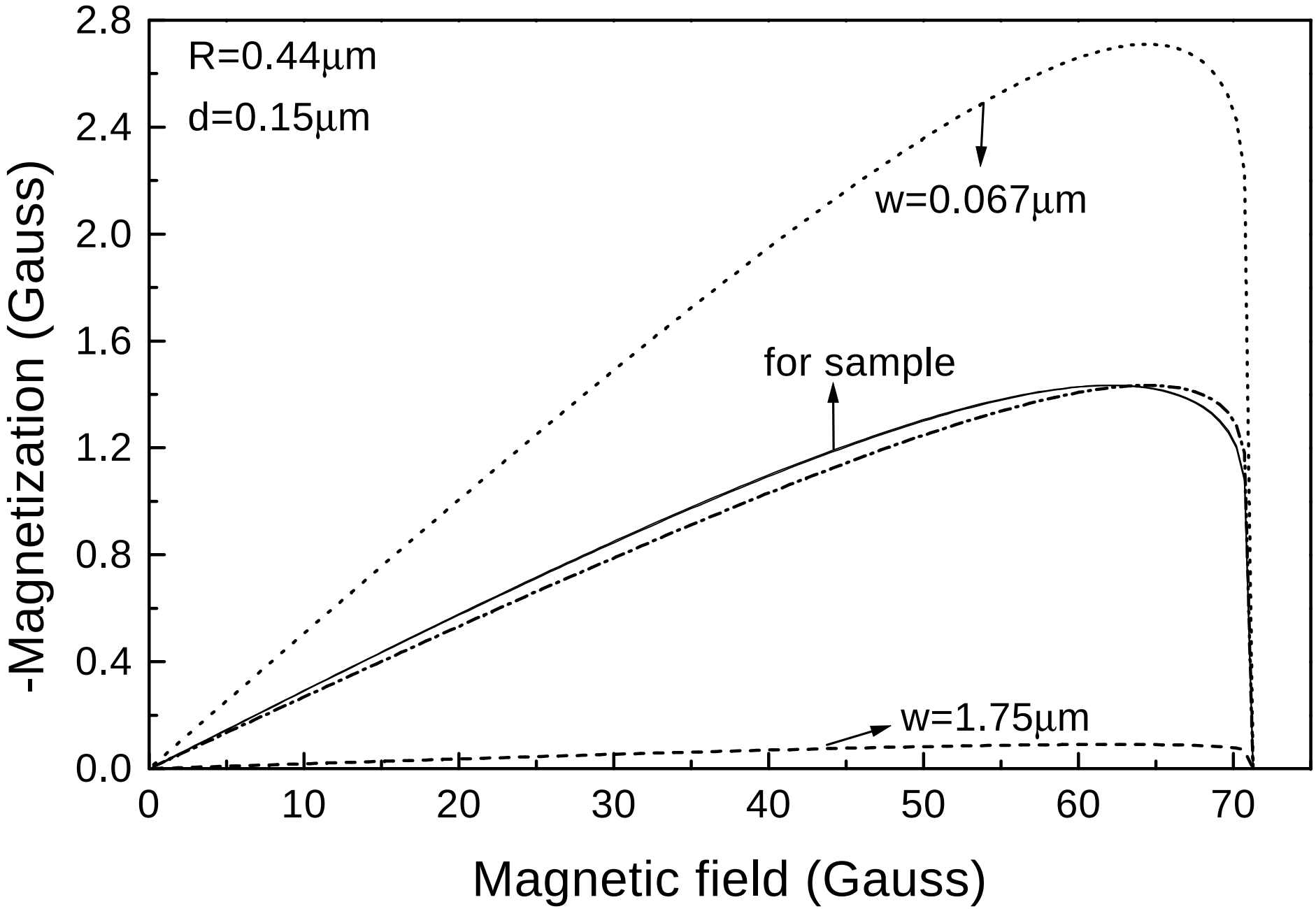
R=0.44μm
d=0.15μm
w=0.067μm
for sample
w=1.75μm
-Magnetization (Gauss)
Magnetic field (Gauss)
0.0
0.4
0.8
1.2
1.6
2.0
2.4
2.8
0
10
20
30
40
50
60
70

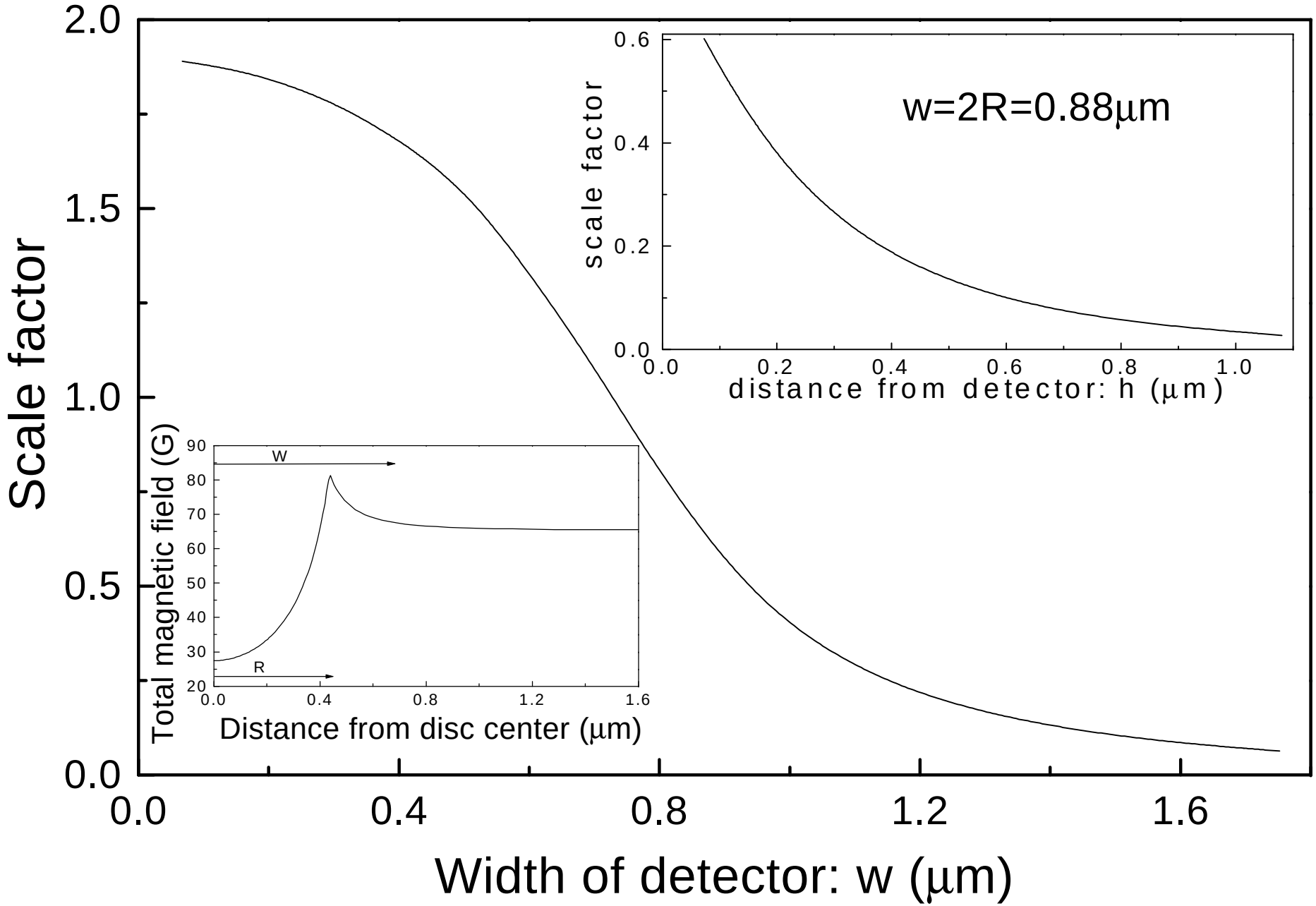
Scale factor
2.0
1.5
1.0
0.5
0.0
0.0
0.4
0.8
1.2
1.6
Width of detector: w (μm)
w=2R=0.88μm
scale factor
0.6
0.4
0.2
0.0
0.0
0.2
0.4
0.6
0.8
1.0
distance from detector: h (μm)
Total magnetic field (G)
90
80
70
60
50
40
30
20
W
R
0.0
0.4
0.8
1.2
1.6
Distance from disc center (μm)

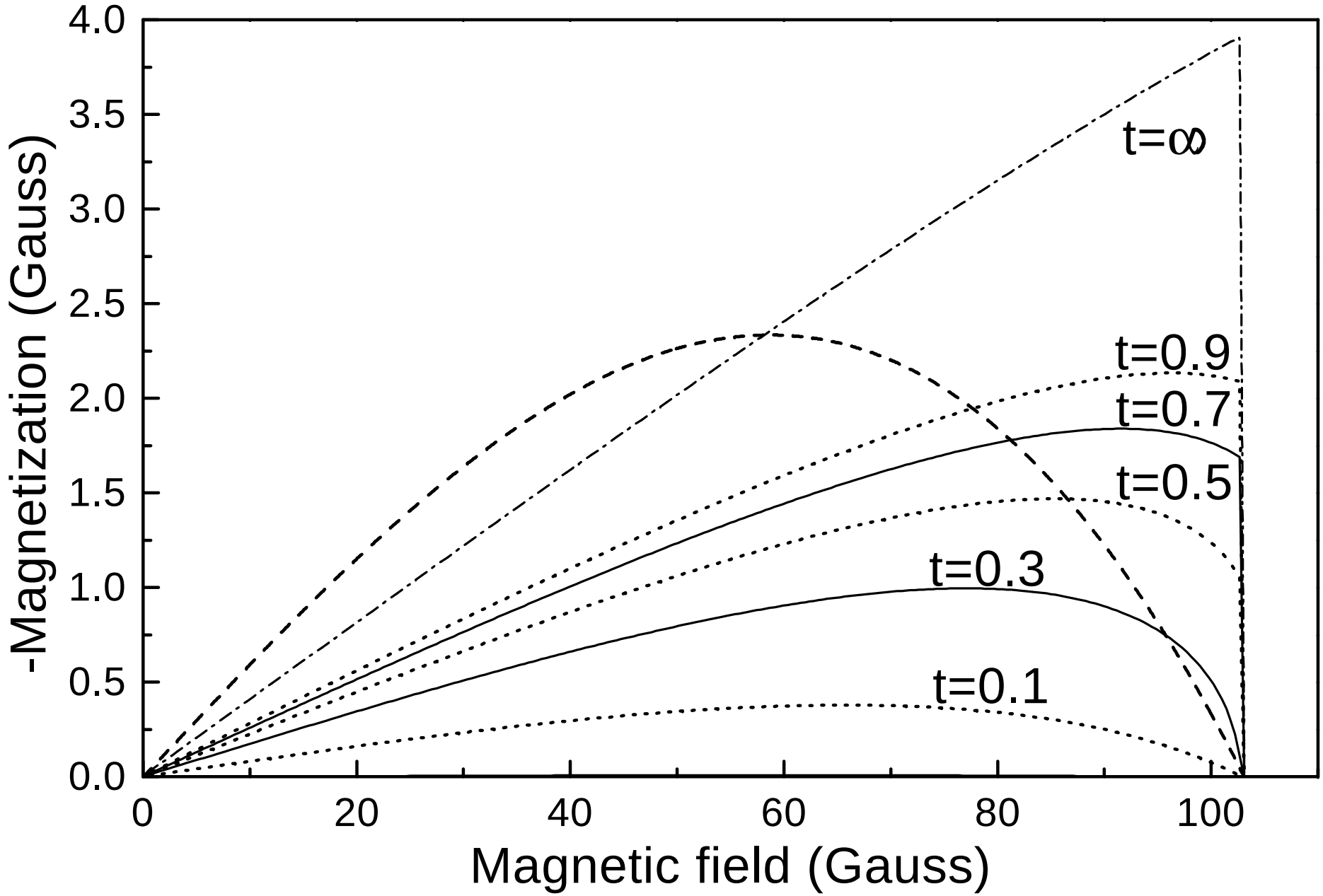
-Magnetization (Gauss)
Magnetic field (Gauss)
0.0
0.5
1.0
1.5
2.0
2.5
3.0
3.5
4.0
0
20
40
60
80
100
t=∞
t=0.9
t=0.7
t=0.5
t=0.3
t=0.1

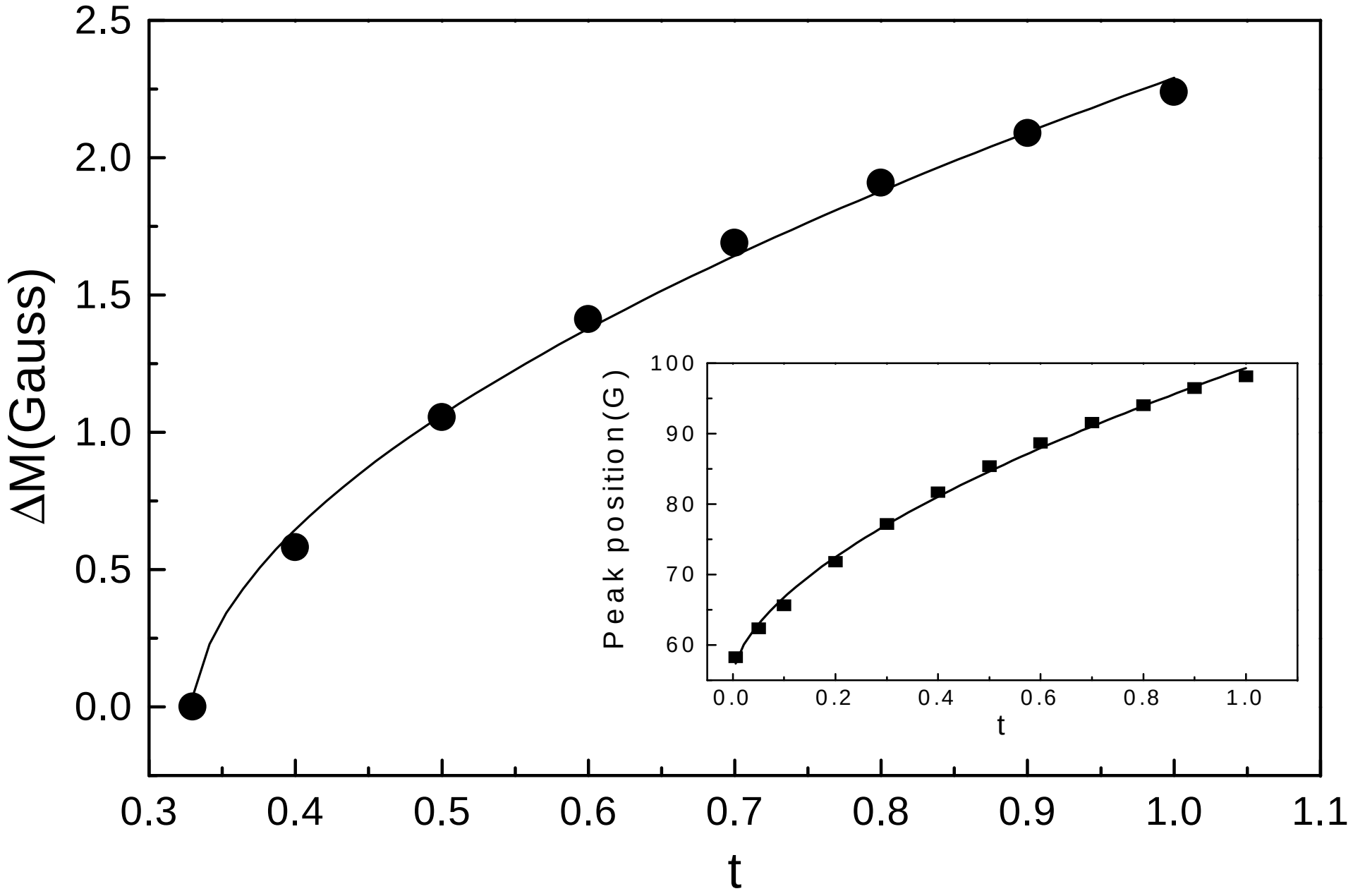
ΔM(Gauss)
2.5
2.0
1.5
1.0
0.5
0.0
0.3
0.4
0.5
0.6
0.7
0.8
0.9
1.0
1.1
t
Peak position(G)
100
90
80
70
60
0.0
0.2
0.4
0.6
0.8
1.0
t

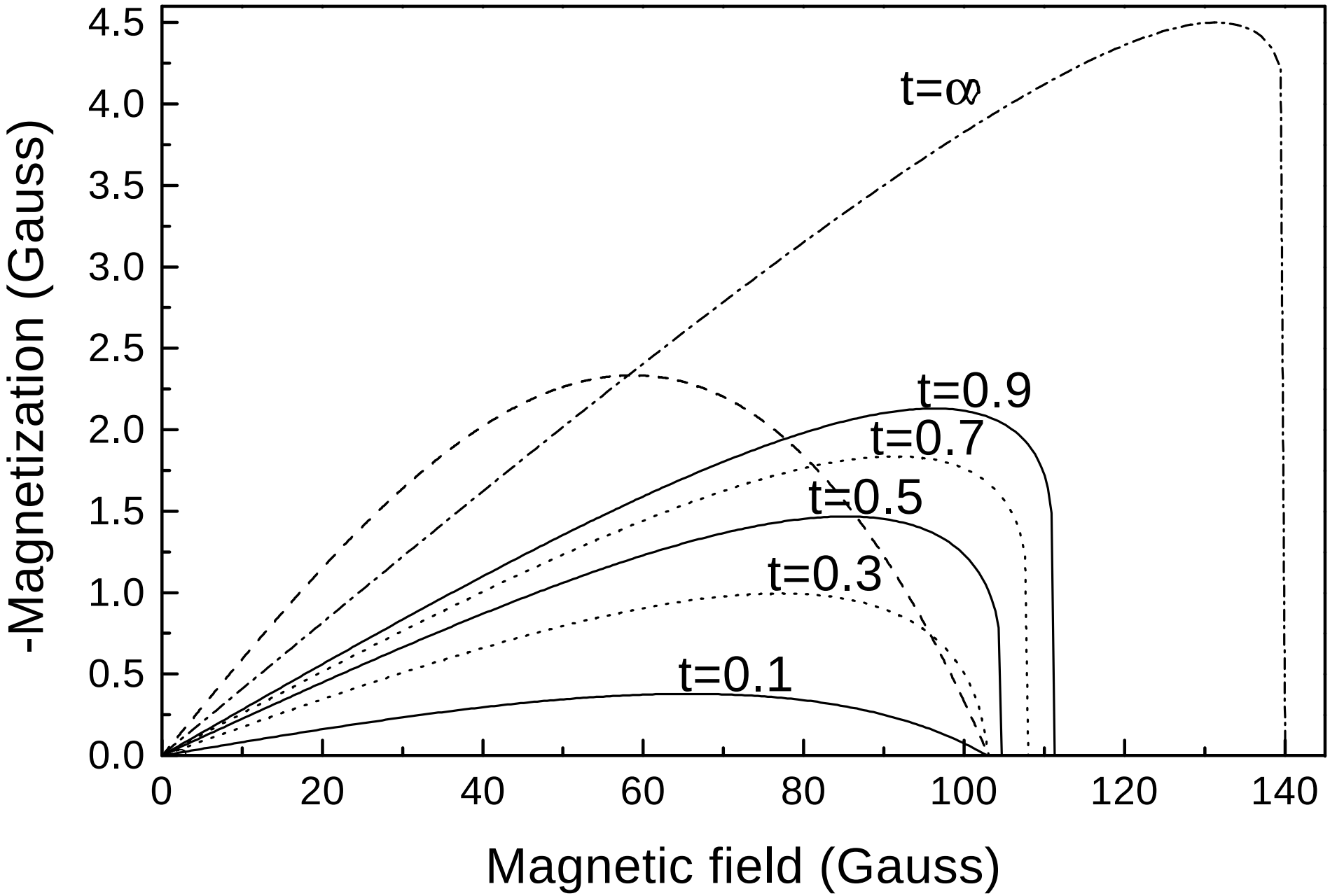
-Magnetization (Gauss)
Magnetic field (Gauss)
0.0
0.5
1.0
1.5
2.0
2.5
3.0
3.5
4.0
4.5
0
20
40
60
80
100
120
140
t=∞
t=0.9
t=0.7
t=0.5
t=0.3
t=0.1

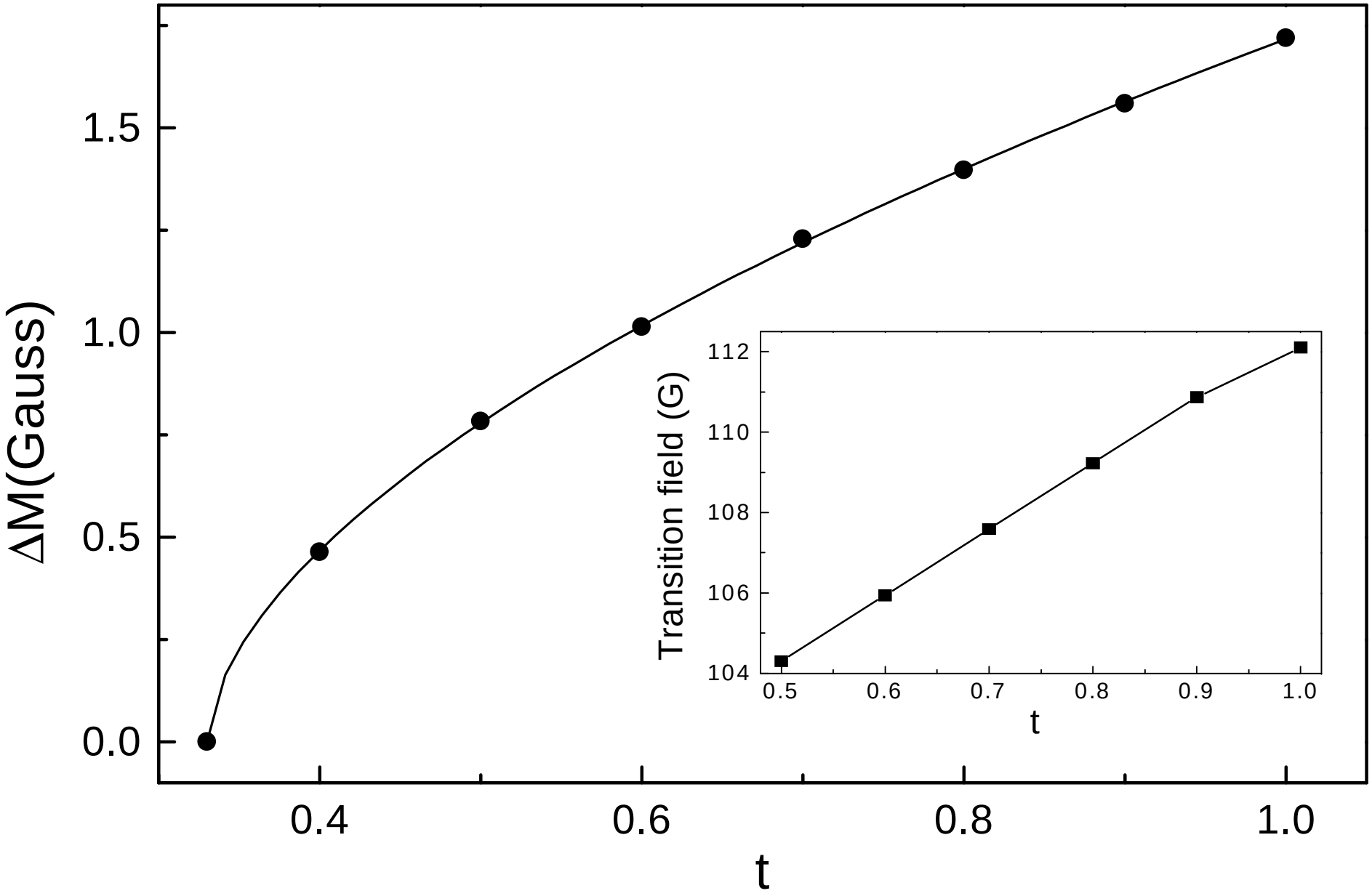
ΔM(Gauss)
1.5
1.0
0.5
0.0
0.4
0.6
0.8
1.0
t
Transition field (G)
112
110
108
106
104
0.5
0.6
0.7
0.8
0.9
1.0
t

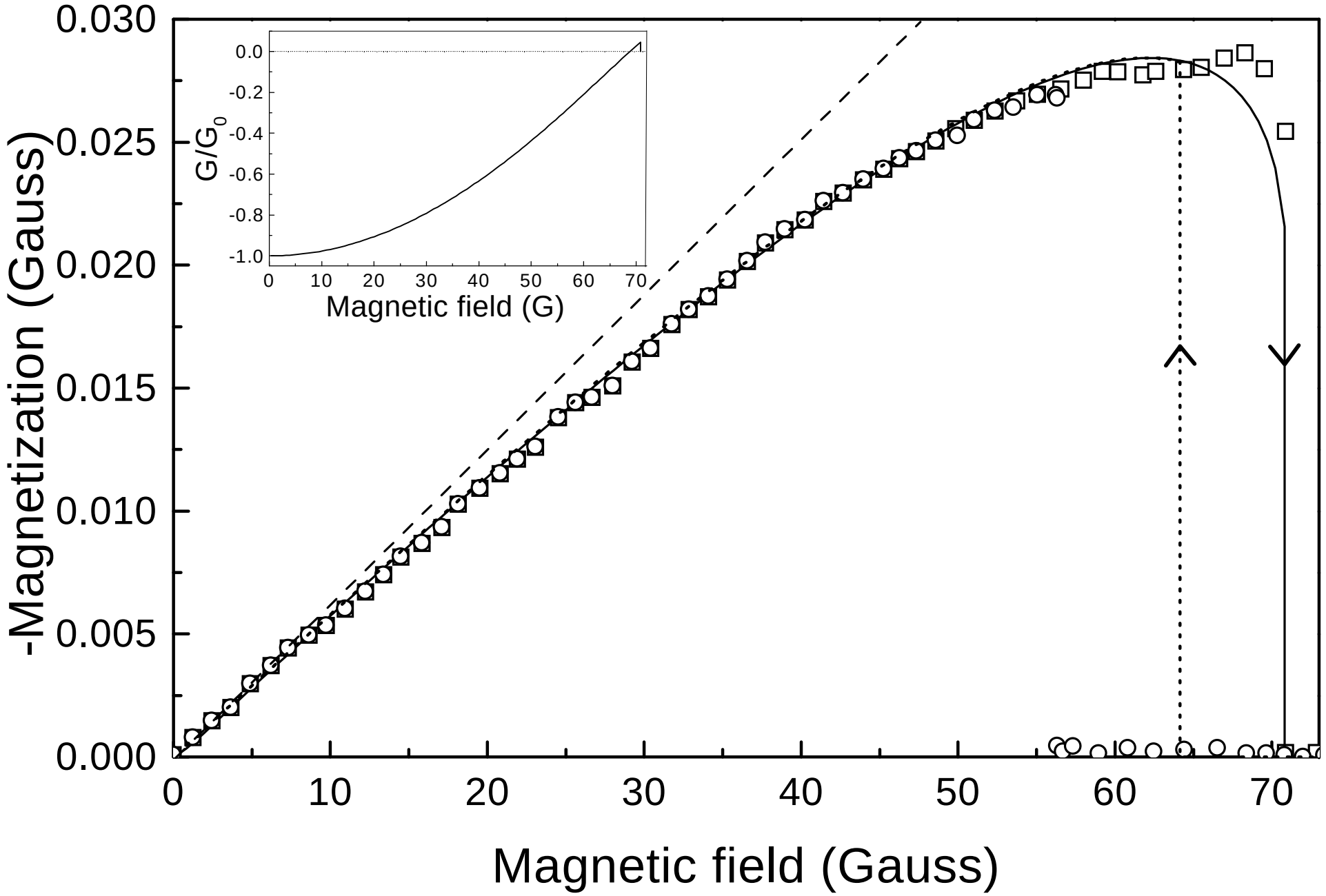
-Magnetization (Gauss)
0.030
0.025
0.020
0.015
0.010
0.005
0.000
0
10
20
30
40
50
60
70
Magnetic field (Gauss)
G/G0
0.0
-0.2
-0.4
-0.6
-0.8
-1.0
0
10
20
30
40
50
60
70
Magnetic field (G)

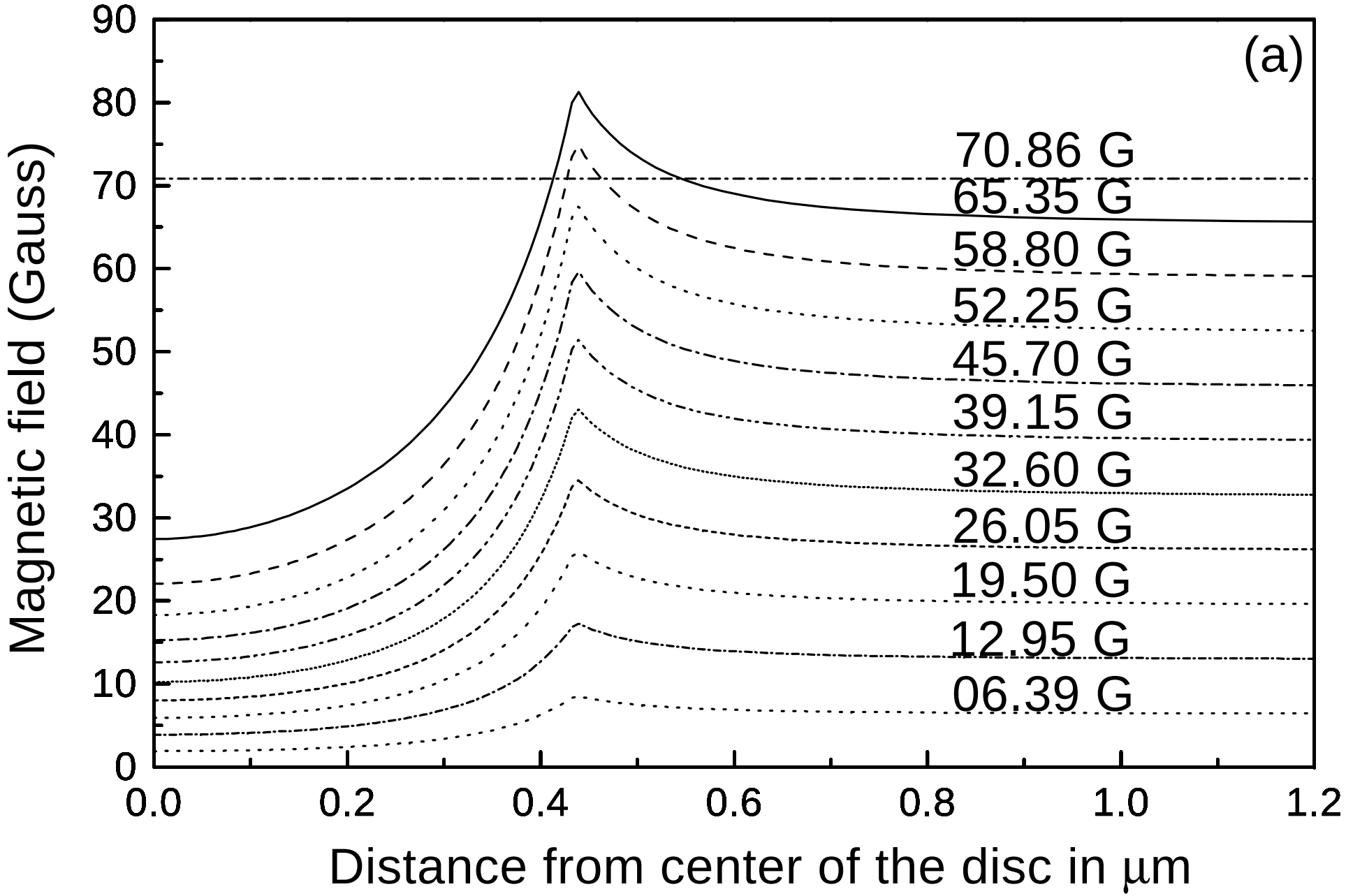
(a)
70.86 G
65.35 G
58.80 G
52.25 G
45.70 G
39.15 G
32.60 G
26.05 G
19.50 G
12.95 G
06.39 G
Magnetic field (Gauss)
Distance from center of the disc in μm
0
10
20
30
40
50
60
70
80
90
0.0
0.2
0.4
0.6
0.8
1.0
1.2

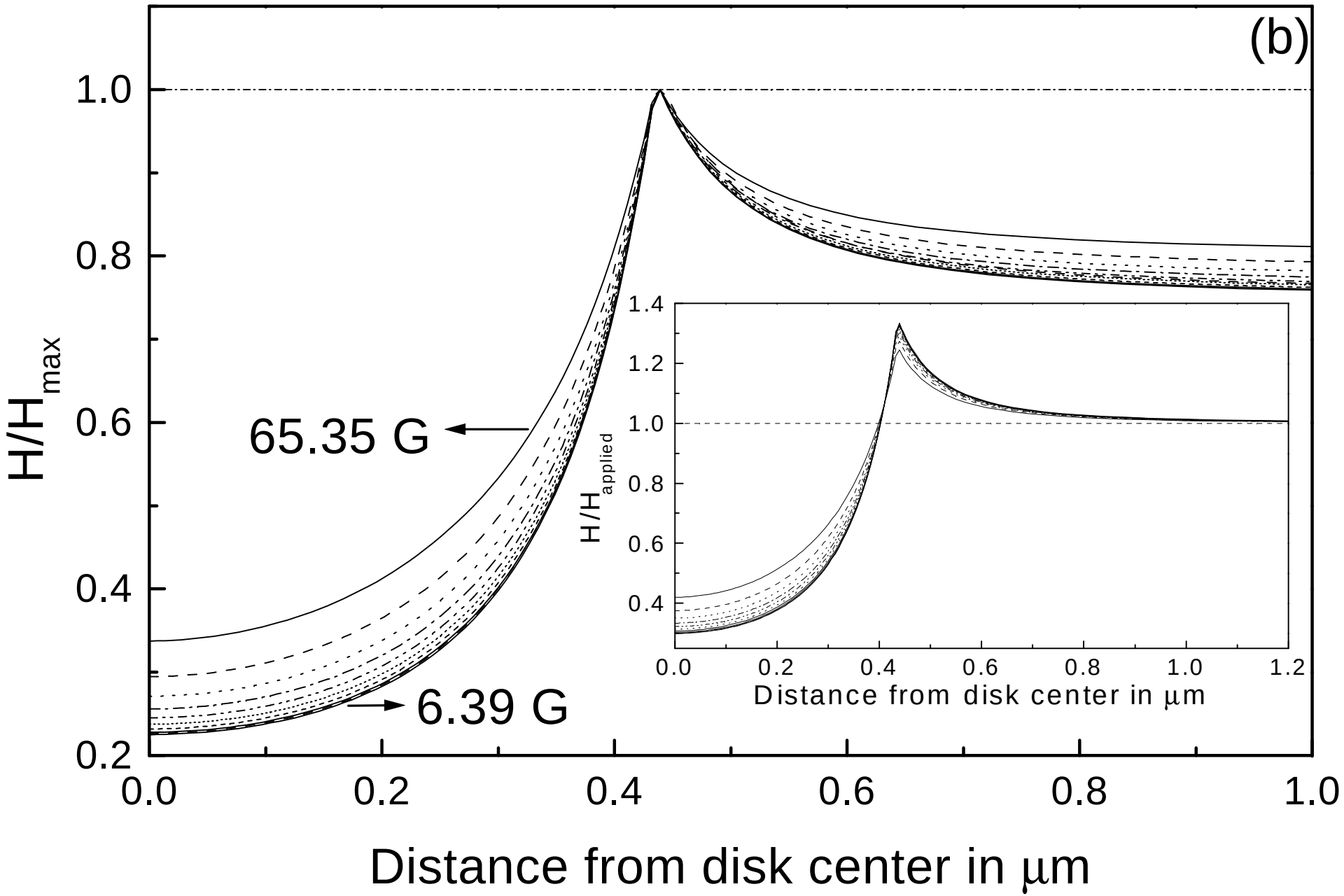
(b)
1.0
0.8
0.6
0.4
0.2
H/H_max
65.35 G
6.39 G
0.0
0.2
0.4
0.6
0.8
1.0
Distance from disk center in μm
1.4
1.2
1.0
0.8
0.6
0.4
H/H_applied
0.0
0.2
0.4
0.6
0.8
1.0
1.2
Distance from disk center in μm

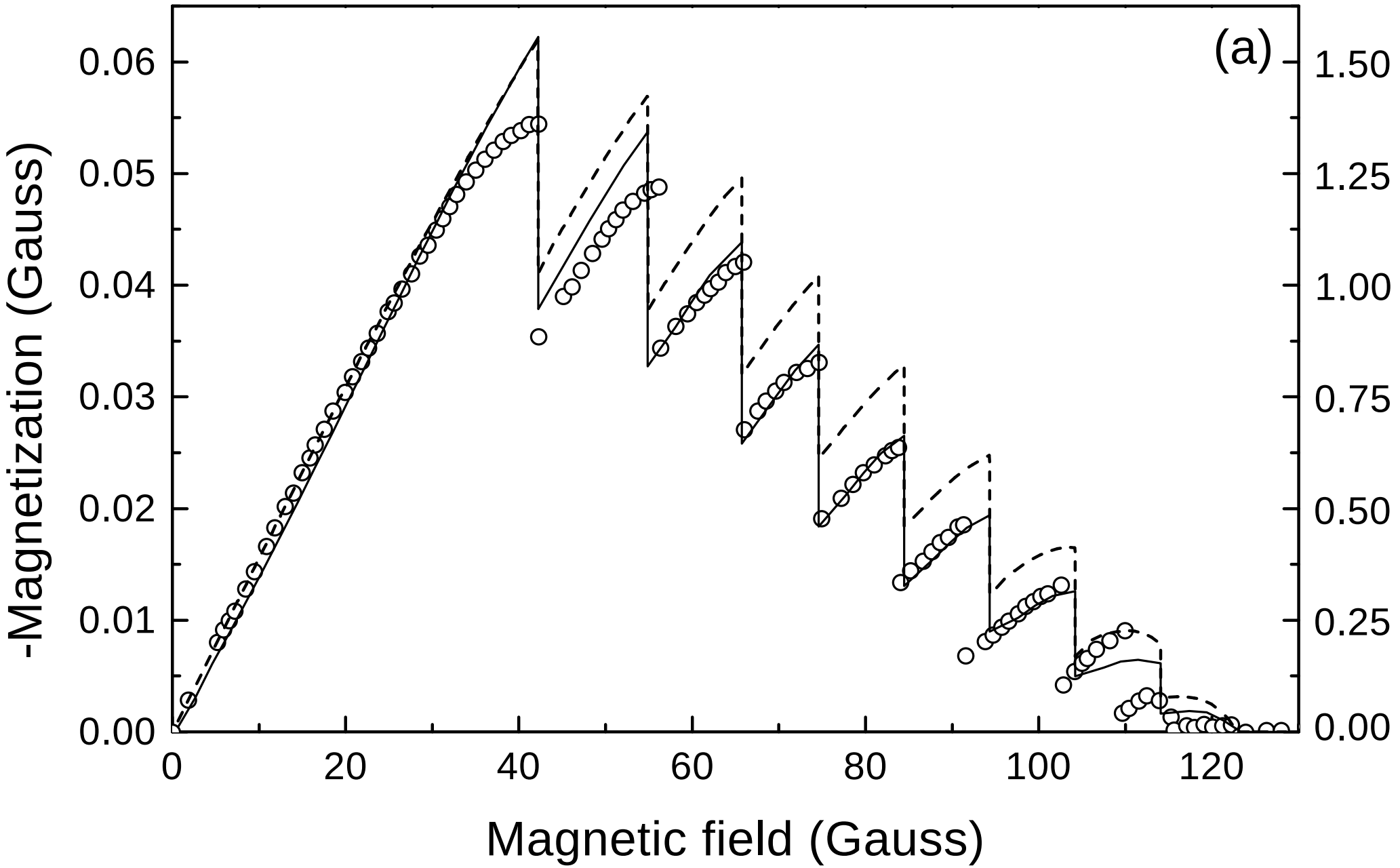
(a)
-Magnetization (Gauss)
0.06
0.05
0.04
0.03
0.02
0.01
0.00
1.50
1.25
1.00
0.75
0.50
0.25
0.00
0
20
40
60
80
100
120
Magnetic field (Gauss)

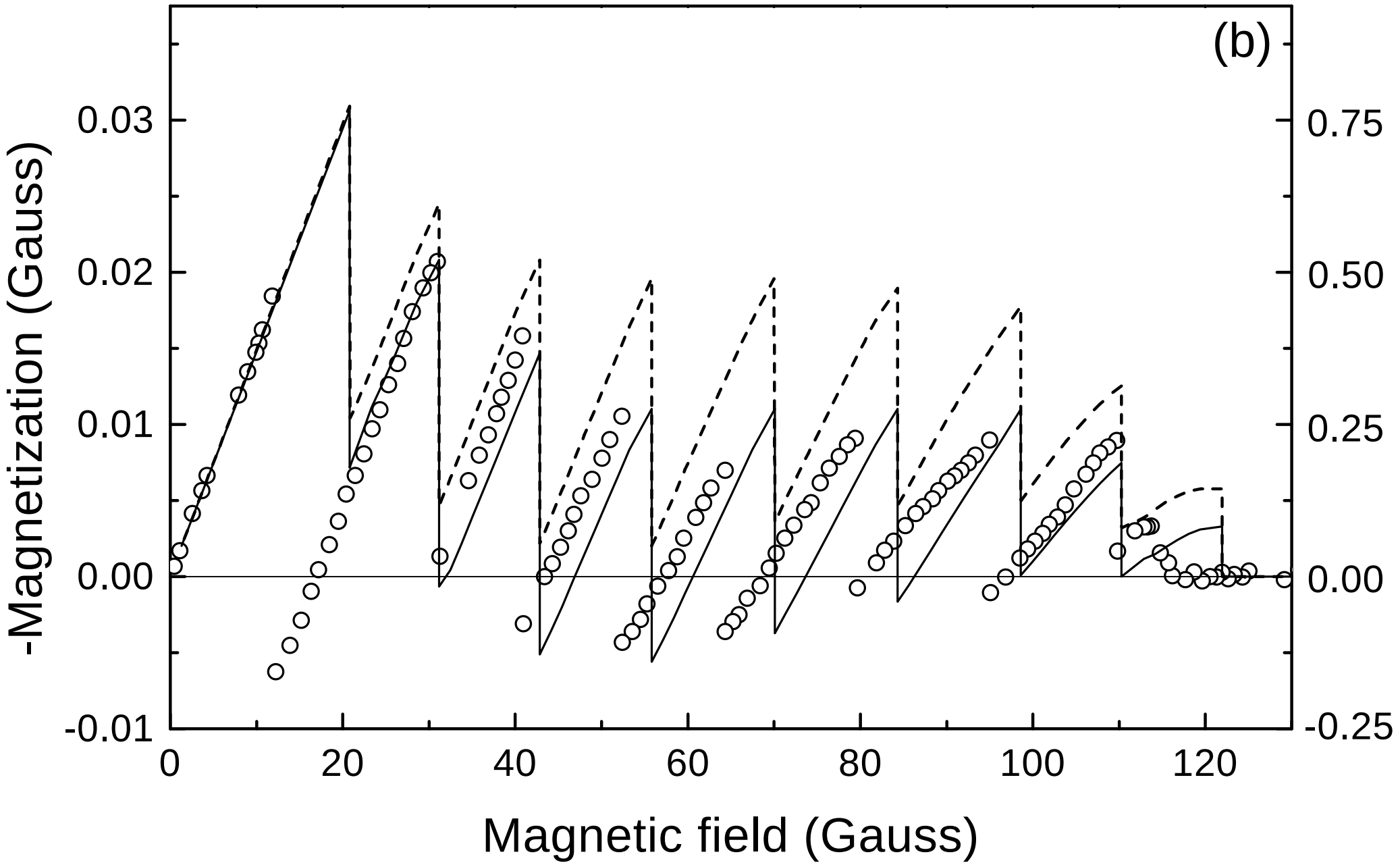
(b)
-Magnetization (Gauss)
0.03
0.02
0.01
0.00
-0.01
0.75
0.50
0.25
0.00
-0.25
0
20
40
60
80
100
120
Magnetic field (Gauss)

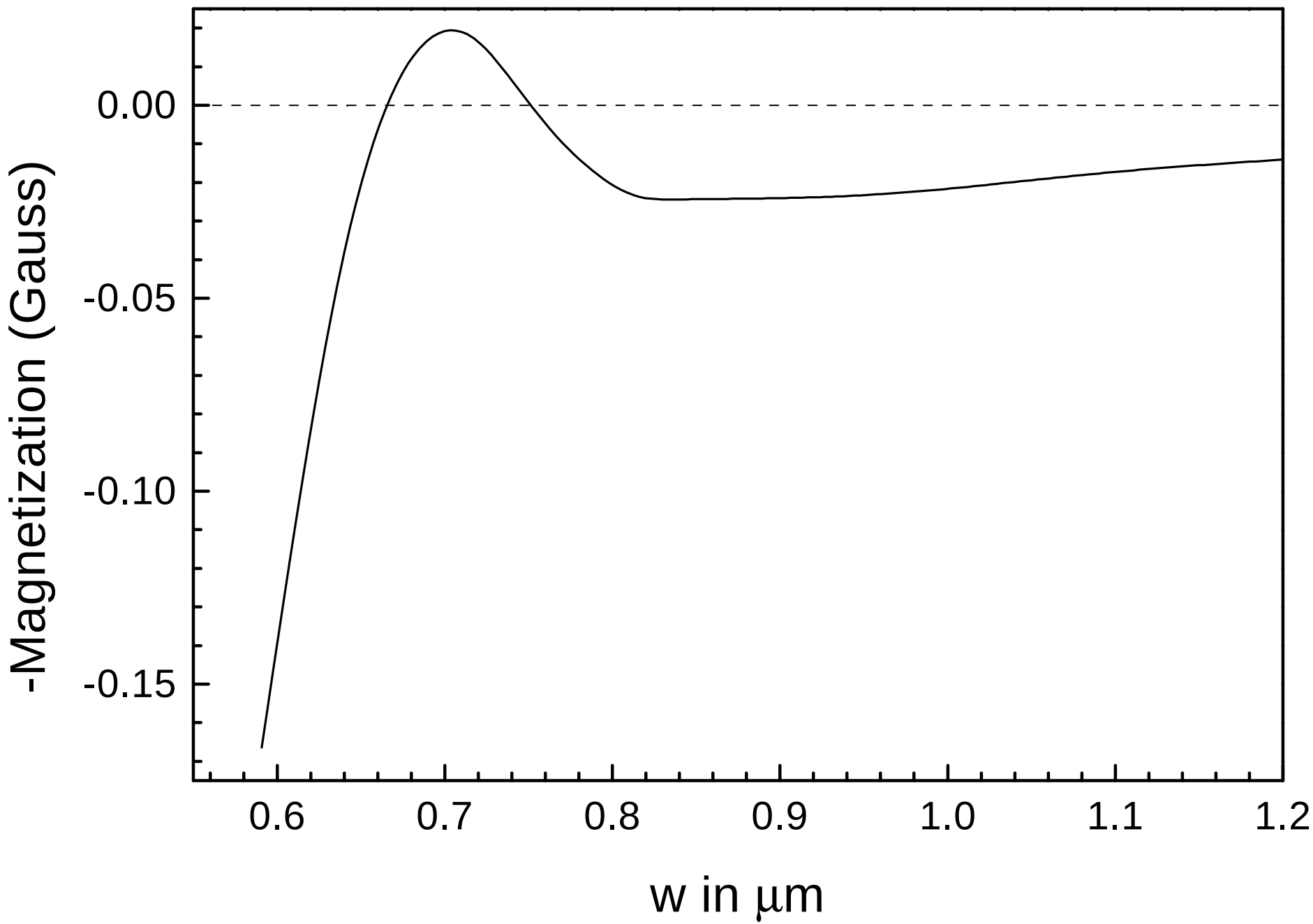
0.00
-0.05
-0.10
-0.15
-Magnetization (Gauss)
0.6
0.7
0.8
0.9
1.0
1.1
1.2
w in μm

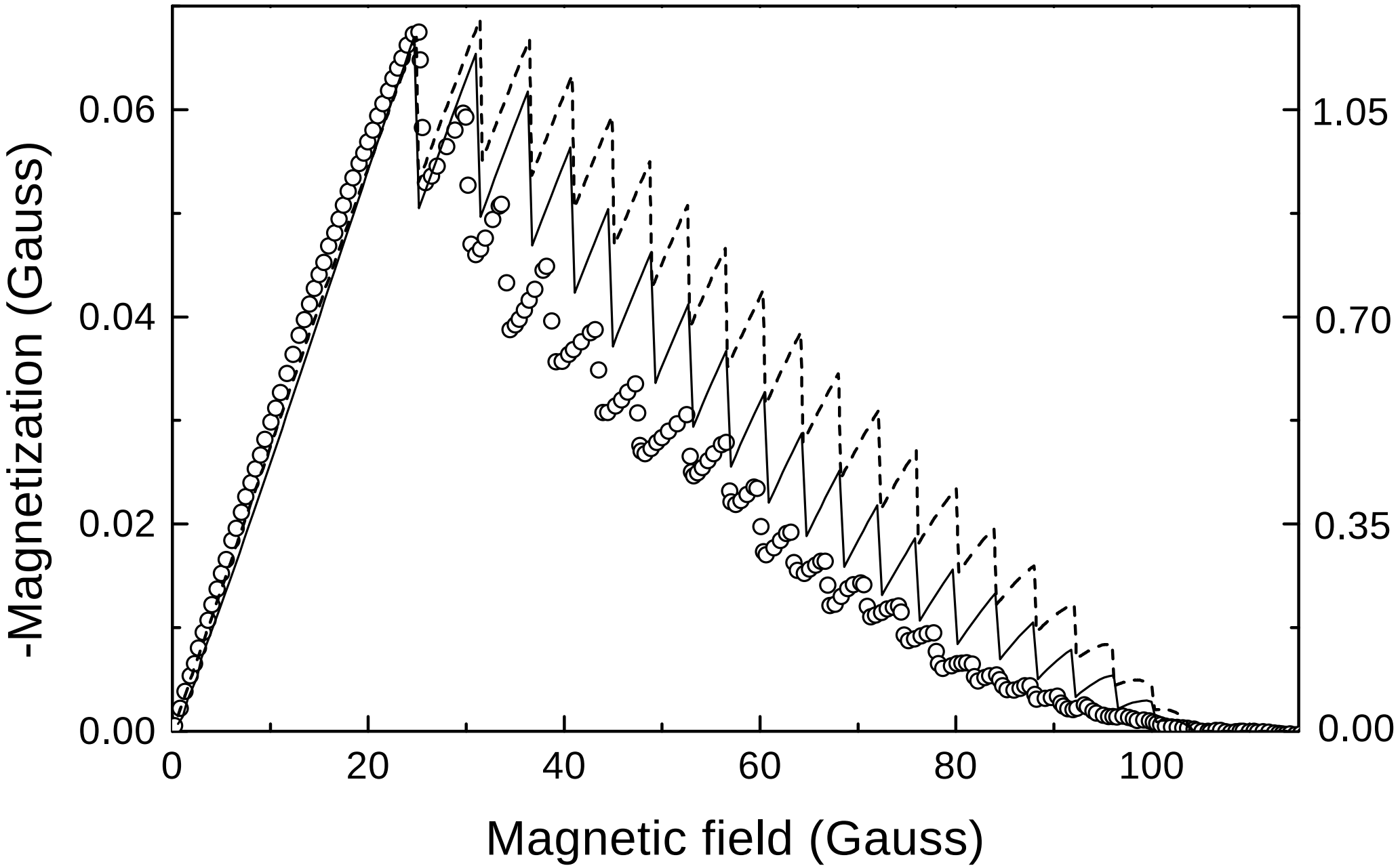
-Magnetization (Gauss)
0.00
0.02
0.04
0.06
0.00
0.35
0.70
1.05
0
20
40
60
80
100
Magnetic field (Gauss)

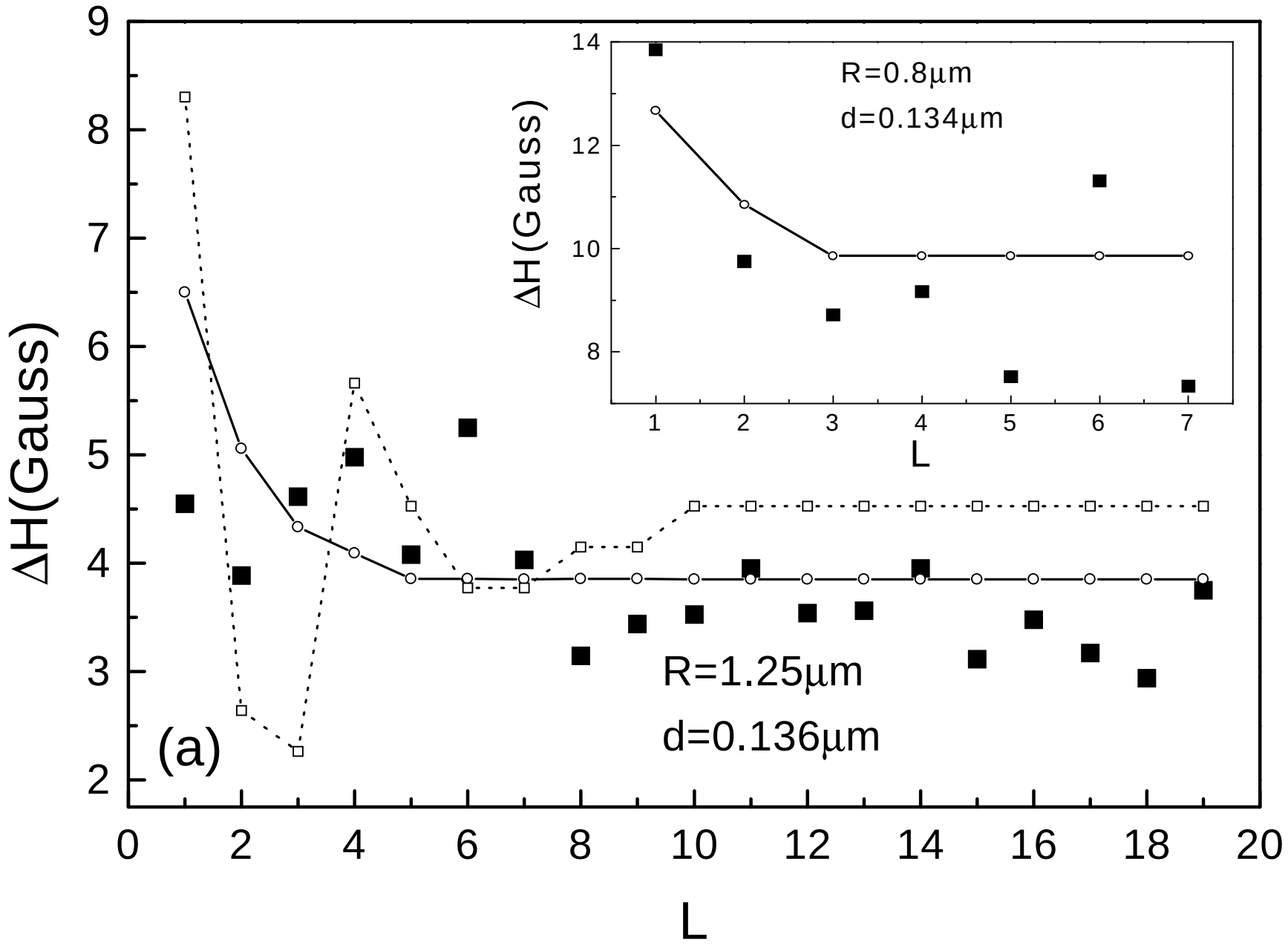
ΔH(Gauss)
L
(a)
R=1.25μm
d=0.136μm
R=0.8μm
d=0.134μm

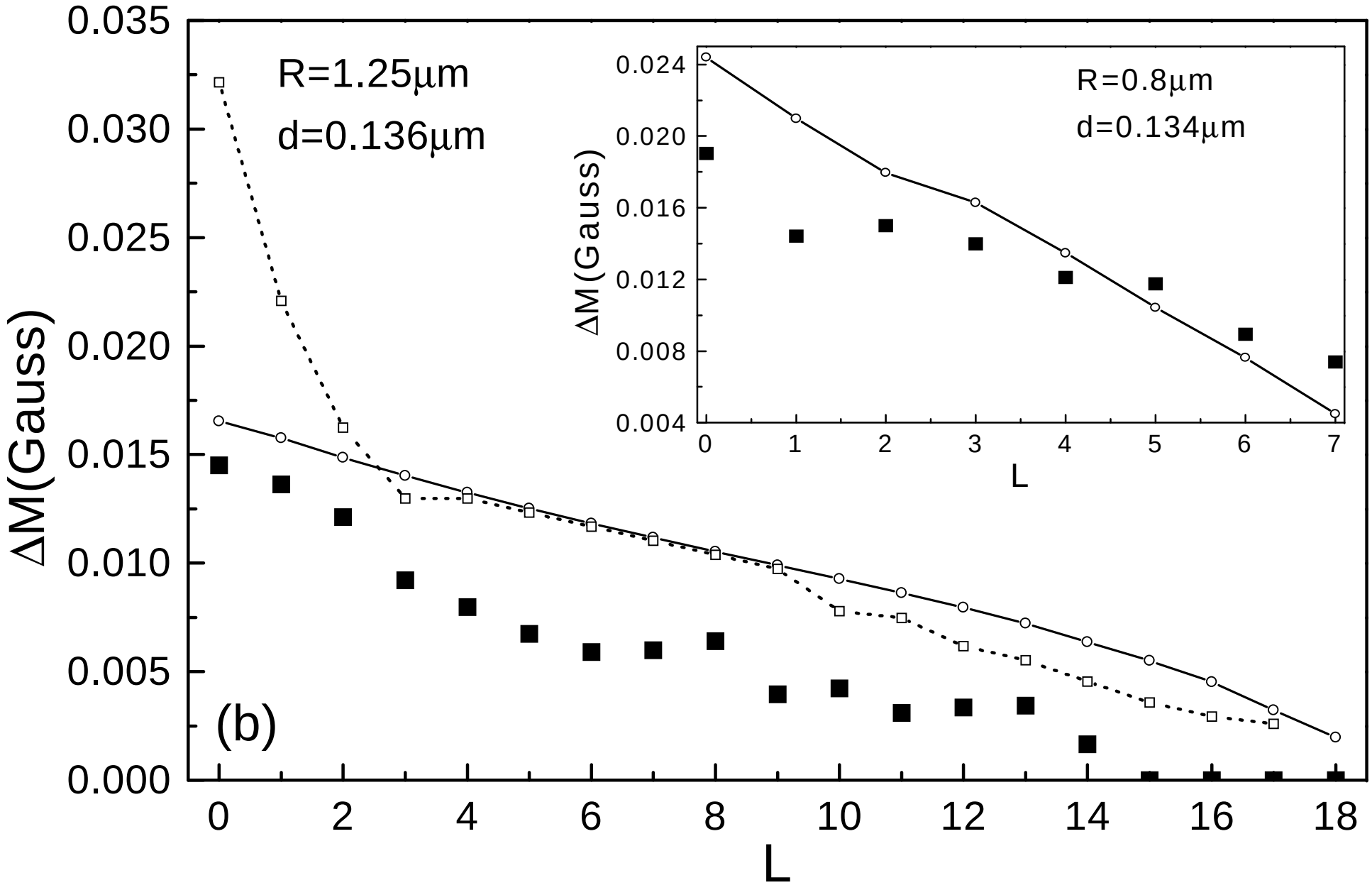
R=1.25μm
d=0.136μm
(b)
ΔM(Gauss)
L
0.035
0.030
0.025
0.020
0.015
0.010
0.005
0.000
0
2
4
6
8
10
12
14
16
18
R=0.8μm
d=0.134μm
ΔM(Gauss)
L
0.024
0.020
0.016
0.012
0.008
0.004
0
1
2
3
4
5
6
7